Impact of solvent dry down, phase change, vehicle pH and slowly reversible keratin binding on skin penetration of cosmetic relevant compounds: II. Solids

Kevin Tonnis[a], Gerald B. Kasting[b], and Joanna Jaworska[c]*

[a]College of Engineering and Applied Science
The University of Cincinnati
Cincinnati, OH USA 45221

[b]The James L. Winkle College of Pharmacy
The University of Cincinnati
Cincinnati, OH USA 45267-0514

[c]The Procter & Gamble Company
Discovery Innovation Platforms
Brussels Innovation Center, Belgium

*Correspondence:

Joanna Jaworska
The Procter & Gamble Company
Brussels Innovation Center
Strombeek-Bever, Belgium
Phone: +32474843034
Email: jaworska.j@pg.com

ABSTRACT

We extended a mechanistic, physics-based framework of the dry down process, previously developed for liquids and electrolytes, to solids and coded it into the latest UB/UC/P&G skin permeation model, herein renamed DigiSkin. The framework accounts for the phase change of the permeant from dissolved in a solvent (liquid) to precipitated on the skin surface (solid). The evaporation rate for the solid is reduced due to lower vapor pressure for the solid state versus subcooled liquid. These vapor pressures may differ by two orders of magnitude. The solid may gradually redissolve and penetrate the skin. The framework was tested by simulating the in vitro human skin permeation of the 38 cosmetically relevant solid compounds reported by Hewitt et al., J. Appl. Toxicol. 2019, 1-13. The more detailed handling of the evaporation process greatly improved DigiSkin evaporation predictions (r^2 = 0.89). Further, we developed a model reliability prediction score classification using diverse protein reactivity data and identified that 15 of 38 compounds are out of model scope. Dermal delivery predictions for the remaining chemicals have excellent agreement with experimental data. The analysis highlighted the sensitivity of water solubility and equilibrium vapor pressure values on the DigiSkin predictions outcomes influencing agreement with the experimental observations.

Keywords:

Absorption, Biophysical models, Dermal delivery, Disposition, Percutaneous, Skin, Transdermal

Abbreviations

BA	benzoic acid
CA	cinnamic acid
CE	Cosmetics Europe
DD	dermal delivery
DE	dermis
DPRA	Direct Peptide Reactivity Assay
ED	viable epidermis
IQ	2-amino-3-methylimidazo[4,5-f]quinoline
IVPT	In vitro permeation test
kDPRA	kinetic modification of Direct Peptide Reactivity Assay
MP	melting point
LLNA	Local Lymph Node Assay
OASIS	OASIS Laboratory of Mathematical Chemistry
PBS	phosphate buffered saline
PPRA	Peroxidase/peroxide-activated Peptide Reactivity Assay
RF	receptor fluid
SC	stratum corneum
SI	Supplementary Information
P_{vp}	vapor pressure
TIMES-SS	Tissue Metabolism Simulator for predicting Skin Sensitization

1. Introduction

Computer simulation of the dermal delivery of topically applied drugs and cosmetics is increasingly used for safety assessments and formulation design as the models mature and their fidelity increases. While skin penetration has been historically measured using in vitro experimentation, limited time and resources prevent these experiments from being performed for all possible chemicals, formulations, environmental conditions, and exposure times. Predictive models for dermal absorption after finite dose application that are rooted both in experiments and the underlying transport phenomena may be used to fill in the gaps between experimental data and lead to better understanding the physics behind exposure due to topical application.

In a recently published report (Tonnis et al., 2022) the transient skin absorption of several chemicals relevant to cosmetic and personal care products was examined using one such model developed within our group, designated therein UB/UC/P&G Model 4 and subsequently renamed Model 4.0 (Tonnis et al., 2024). Following internally developed nomenclature within Procter & Gamble, we will henceforth refer to the gPROMS implementation of this model as DigiSkin 4.0. This model, a derivative of the original UB/UC model (Dancik et al., 2013), included the ability to handle highly polar and ionized solutes (Kasting et al., 2019; Yu et al., 2021; Yu et al., 2022), the ability to simultaneously model the behavior or a solute and solvent during dry down (Yu et al., 2022), and slowly reversible keratin binding kinetics (Nitsche and Kasting, 2022). DigiSkin 4.0 predictions were assessed using a test dataset taken from the recent finite dose skin penetration study by Hewitt et al (Hewitt et al., 2019). This study comprises one leg of a three-part study of 56 cosmetic relevant compounds commissioned by the Cosmetics Europe ADME Task Force. The

other two legs provided physical properties measurements (Grégoire et al., 2017) and steady state partition coefficients and skin permeability coefficients for each of the chemicals (Ellison et al., 2020). We will refer to this dataset collectively as the "CE dataset". The Tonnis et al. 2022 study focused on the subset of those compounds that were liquids in their neat state at 32^{o}C, the skin temperature in the experiments. This subset was selected based on the phase state of the neat solutes because of complications that arise when the solute precipitates after the solvent has evaporated. The physical and chemical properties of a solid change considerably more when precipitating from a solvent than those of a liquid (Anissimov and Roberts, 2001; Scheuplein and Ross, 1974; Yu et al., 2021). A delay in penetration due to the dissolution of precipitated solids has been shown to be a feature of the CE data set (Hamadeh et al., 2021). A previous analysis of the CE dataset using the UB/UC model (Gregoire et al., 2021), therein called the CDC model, showed overpredicted evaporation rates. By calibrating the overall evaporation mass transfer coefficient employed by the model to account for the experimental setup, DigiSkin 4.0 was generally able to accurately predict the dermal delivery of the CE liquids (Tonnis et al., 2022).

Solvent-deposited solids add an additional degree of complexity to the dermal absorption picture, as absorption may in some cases be dissolution-limited. In (Yu et al., 2022) we handled this distinction in a binary fashion, introducing the concept of "hard" and "soft" solids. We subsequently extended this model in (Tonnis et al., 2024) to provide a continuous range of dissolution rates and to also include keratin binding and the possibility that the deposited solid might be a weak electrolyte in an arbitrary stage of ionization. In the present study, we extend the analysis to the rest of the CE dataset and implement additional features necessary for handling a wider range of precipitated solids.

2. Mathematical model

The skin disposition model employed in this study builds on a one-dimensional model developed by our group on the gPROMS® platform to predict the transient absorption and evaporation rates of a binary solute/solvent combination applied to the skin (Yu et al., 2021; Yu et al., 2022). The model comprises a vehicle layer, three skin layers and a follicular pathway in parallel with the composite skin pathway. Table 1 summarizes recent developments leading up to the present model, DigiSkin 4.2. DigiSkin 4.2 implements all the changes through (Tonnis et al., 2024) and also makes some new distinctions. Significant differences from the CE liquids analysis are described in this section. The nomenclature is that of (Yu et al., 2022); thus, the overbars introduced in (Tonnis et al., 2022) to carefully distinguish macroscopic, microscopic and ultrascopic properties associated with the stratum corneum layer have been omitted. These levels of homogenization can alternatively be recognized as follows: a subscript containing “sc” denotes a macroscopic property, one containing “lip” or “cor” denotes a microscopic property, and one containing “ker” denotes an ultrascopic property associated with the reversible binding of solutes to keratin microfibrils. The ultrascopic relationships do not appear below as the treatment of keratin binding is identical to that in (Tonnis et al., 2022) (where the “ker” designations appeared as superscripts). For details of the slowly reversible binding treatment we refer the reader to Sects. 2.1, 4.2 and 5.2 of the Tonnis et al. paper.

Table 1

Summary of the development of the DigiSkin model

Model	Major Added Features	New Functionality	Reference
UB/UC	One dimensional 3-layer skin penetration model with vehicle.	Simulation of finite dose skin penetration experiments for moderately lipophilic compounds.	Dancik et al. 2012
Model 1	Polar pathway through the SC lipids added to the composite SC matrix. Follicular pathway added in parallel to the composite SC.	Improved predictions for steady-state permeability of hydrophilic compounds. Improved representation of the physical structure of skin.	Kasting et al. 2019
Model 2	Transient equations for a polar pathway developed. Instant evaporation of volatile solvents replaced by a transient solvent dry down process.	Improved predictions for transient permeability of hydrophilic compounds. Allows simulation of simple vehicle dry down and incorporation of vehicle-skin interactions.	Yu et al. 2021
Model 3	Depth-dependent lag time added to the follicular pathway. Surface roughness of the SC added to regulate solute transport into the infundibulum. Dissolution limitation for solvent deposited solids incorporated into model.	Burst effect due to outer root sheath permeability reduced to better represent experimental observations. Solute no longer accumulates in follicles after solvent dry down. The deposited solid dissolution rate can be determined from finite dose data.	Yu et al 2022
DigiSkin 4.0	Mechanistic framework for liquids permeation in leave on applications. Equilibrium binding to keratin within the SC replaced by slowly reversible binding.	Predicted SC and receptor solution amounts in transient simulations are more consistent with a SC reservoir.	Tonnis et al 2022
DigiSkin 4.1	Mechanistic framework for weak electrolytes permeation in free or salt form developed. Transient SC and vehicle pH drift implemented.	pH drifts post-dose follow SC surface measurements. pH dependence of permeation of solvent deposited solids is refined.	Tonnis et al 2024
DigiSkin 4.2	Improved mechanistic framework for weak electrolytes permeation in leave on applications. Solid solute evaporation model includes distinction between subcooled liquid VP and neat solid VP. Model for pH drift after application of weak electrolytes extended to solutions buffered to any pH. Digiskin prediction reliability score developed based on potential to covalently bind to SC proteins.	VP changes of a solid solute during dry down more accurately represented. More accurate simulation of electrolytes dosed in buffered solutions. Identification out of model scope compounds enabled.	Present

2.1 Dissolution limitation

After a volatile solvent evaporates from a binary solution, it may leave a solid precipitate on the SC surface. Continued penetration of the solid is limited by its dissolution into and permeation rate through a thin boundary layer at the SC surface. In DigiSkin 3 (Yu et al., 2022), the boundary layer was considered to be comprised of skin surface film lipids (for in vivo exposures, cf. (Stefaniak and Harvey, 2006)) or SC intercellular lipids (for in vitro exposures employing thoroughly washed skin). The absorption rate was quantified using a one-layer diffusive mass transfer model in which the dissolution rate is proportional to the lipid solubility, S_{lip}, of the precipitated permeant less the SC surface concentration. The flux of permeant into the top layer of the SC was given by

$$J(0,t) = \kappa_{lip}\left[S_{lip} - K_{lip/sc}C_{sc}(0,t)\right] \quad (1a)$$

$$= \kappa_{lip}[K_{lip/w}S_w - (\frac{K_{lip/w}}{K_{sc/w}})C_{sc}(0,t)] \quad (1b)$$

where Eq. (1b) results from the assumption that the value of $K_{lip/w}$ is independent of concentration. Here κ_{lip} is the interfacial mass transfer coefficient, $K_{lip/w}$ is the lipid/water partition coefficient, S_w is the solubility in water, $K_{sc/w}$ is the SC/water partition coefficient, and C_{sc} is the freely diffusing solute concentration in the SC. For in vitro studies, (Yu et al., 2022) proposed that κ_{lip} could be estimated as

$$\kappa_{lip}^{in\ vitro} = \frac{k_{trans}\delta}{\delta_{lip}} f_{contact} f_{thermo} \quad (2)$$

where $k_{trans}\delta \cong D_{lip_{trans}}$ is the transverse diffusivity in the film, δ is the width of a single SC lipid bilayer (13 nm), δ_{lip} is the thickness of the lipid layer, $f_{contact}$ is the fractional area of contact of

the deposited solute per unit area of skin and f_{thermo} is a thermodynamic factor compensating for nonideal properties of the solution including self-association of the solute, which led to concentration-dependent values of $K_{lip/w}$ for the solutes in (Yu et al., 2022). In the absence of specific data on nonideal solutes, we set f_{thermo} = 1 for the present analysis.

In the present analysis, as well as for results reported recently by (Miller and Kasting, 2022), there is a need to explain the fact that organic solutes deposited on skin as salts may continue to penetrate into the skin despite the poor lipid solubility of the salt. We addressed this problem for the Miller & Kasting data in (Tonnis et al., 2024) by allowing slow interconversion of free acids and bases with their salts as the SC recovers to its natural pH. Here we re-apply this feature to the weak electrolytes in the CE solids dataset.

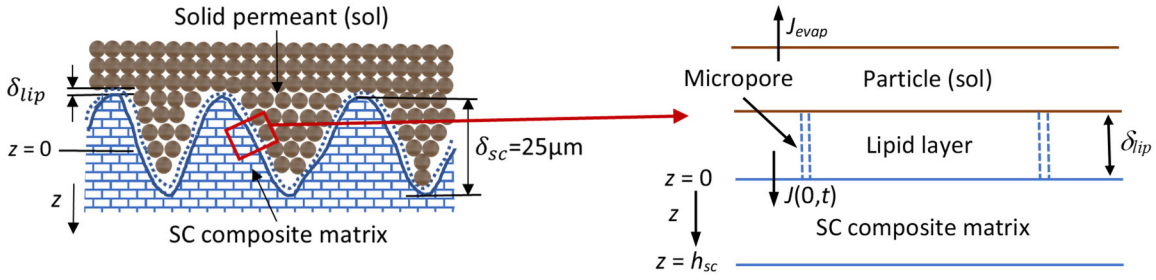

Fig 1. Schematic diagram of the SC surface covered with a layer of deposited particles, adapted from Yu et al., 2022. Particles are in direct contact with a lipid layer, which may be sebum for in vivo exposures, but is considered to be SC lipids for in vitro exposures in which the skin surface has been thoroughly washed. The lipids have defects or micropores as in the SC composite matrix that are considered the likely pathways for proton transfer from the SC, leading to gradual neutralization of deposited weak electrolyte salts.

(Yu et al., 2022) argued that a fully hydrated skin condition was appropriate for bench top exposures involving PBS donor solutions in the CE in vitro permeation study (Hewitt et al., 2019). We conducted the solids analysis using this approximation. Thus, the value of k_{trans} was estimated as

$$\log_{10}[k_{trans}, \mathrm{m/s}] = -2.730 - 0.792\mathrm{MW}^{1/3} \quad (3)$$

where MW is the molecular weight. The boundary conditions at the vehicle/lipid and lipid/SC interfaces can be expressed in terms of the flux through the interfacial film as well as the evaporative flux and flux into the SC. For a dissolved solute (Yu et al., 2022)

$$\frac{dM_{surf}}{dt} = -J_{evap} - J\left(-\delta_{lip}, t\right) \quad (4)$$

$$-D_{sc}\frac{\delta C_{sc}(z,t)}{\delta z}|_{z=0} = J(0,t) \quad (5)$$

where $J_{evap} = k_{evap}\,\rho$ is equal to the evaporation flux shown in Fig. 1. The factor k_{evap} depends upon solute vapor pressure and molecular weight as well as air velocity as given in Eqs. (16) and (17) of (Yu et al., 2022). We assume the interfacial film is thin enough that steady state transport through it is rapidly reached, giving $J\left(-\delta_{lip}, t\right) = J(0,t)$. The flux into the SC is calculated in Models 4.1 and 4.2 in the same manner as in Model 4.0. The changes to evaporation flux for a solid are described in the next section.

2.2 Solids evaporation

In Models 2, 3 and 4.0, a permeant may evaporate while dissolved in the vehicle, after precipitating on the surface of the skin, or from the top layer of the SC when the skin is free from material on the surface. Beginning in Model 3, the evaporation of precipitated solids, $P_{vp,sol}$, was distinguished from that of liquids, $P_{vp,liq}$, according to the relationship given by (Haftka et al., 2006), i.e.

$$\ln\left(\frac{P_{vp,liq}}{P_{vp,sol}}\right) = \frac{\Delta S_f}{RT}\left(T_f - T\right) \quad (6)$$

where $\Delta S_f = \Delta H_f / T_f$ is the entropy of fusion, ΔH_f is the enthalpy of fusion, *R* is the universal gas constant, T_f is the melting point in Kelvin, and *T* is the skin temperature in Kelvin. When ΔS_f was unknown, it was estimated as 56.5 J K^{-1} mol^{-1} following Walden's rule (Yalkowski, 1980).

As noted by Grain (Grain, 1990) and many others, Eq. (6) can lead to large errors in estimating the vapor pressure of polar or high melting solids. We found the CE solids analysis to be highly sensitive to the input values of both $P_{vp,liq}$ and $P_{vp,sol}$. After comparing several alternatives we settled on the following scheme: (1) Tabulate predicted values of $P_{vp,sol}$ and $P_{vp,liq}$ at 25°C and 32°C from MPBPWin Vers. 1.44 module in EpiSuite (US_EPA, 2011). $P_{vp,sol}$ estimates are based on the modified Grain method (Stock et al., 2004; Woodrow et al., 2001), whereas $P_{vp,liq}$ estimates are the average of Antoine (Stock et al., 2004) and Grain (Grain, 1990) methods. (2) Replace predicted values with experimental values when available. Experimental values were taken from EpiSuite, CompTox (US_EPA, 2024) and recent literature. (3) adjust experimental values reported at 25°C to 32°C using the ratio of EpiSuite predicted values at those temperatures. Final P_{vp} values used for the simulations are given in Table S2 of the SI. More discussion can be found in Sect. 5.2.1.

2.3 Weak electrolytes

DigiSkin 4.1 and 4.2 handle ionizable compounds similarly to Model 4.0 except in the manner the pH of the SC is determined. In Model 4.0, the SC pH was held constant at 5.5, the default natural pH of the SC. In DigiSkin 4.1 and 4.2, because the dose solution (or vehicle) is in intimate contact with the SC and may temporarily overwhelm its buffer capacity (Miller and Kasting, 2022), the pH of the SC immediately after dose application (pH_{sc}^{0}) is set to that of the vehicle

(pH_{veh}^{0}). Here the superscript "0" represents time post-dose. Over time, both values are allowed to gradually return to the natural SC pH, herein designated $\mathrm{pH}_{\mathrm{sc}}^{\infty}$, according to the relationship

$$\mathrm{pH}_{veh}(t) = \mathrm{pH}_{sc}(t) = \mathrm{pH}_{\mathrm{sc}}^{\infty} + \Delta\mathrm{pH}^{0} \cdot e^{-k_r t} \quad (7)$$

where

$$\Delta\mathrm{pH}^{0} = \mathrm{pH}_{veh}^{0} - \mathrm{pH}_{\mathrm{sc}}^{\infty}. \quad (8)$$

The exponential recovery rate constant, k_r, is calculated as (Tonnis et al., 2024)

$$k_r = \frac{a_0 \beta_{sc}}{\beta_{dose}}. \quad (9)$$

where β_{dose} is the buffer capacity of the dose and β_{sc} is that of the SC. (Tonnis et al., 2024) recommended the values a_0 = 2 h^{-1} and β_{sc} = 10 nmol cm^{-2}, yielding a composite value $a_0\beta_{sc}$ = 20 nmol cm^{-2} h^{-1}, and also provided details on how to calculate β_{dose}. After the aqueous solvent has dissipated from the surface, the precipitated solids are no longer treated as in intimate contact with the SC. Stratum corneum pH (pH_{sc}) continues to evolve according to Eq. (7), but vehicle pH (pH_{veh}) becomes a function of the rates of evaporation and penetration of the deposited free electrolyte and its salt. Details as to how DigiSkin 4.1 and 4.2 handle the boundary conditions on the surface during the stage of dry down when a free electrolyte and its salt are deposited on the skin surface are given in (Tonnis et al., 2024).

3. Methods

3.1 Experimental dataset

The test compounds were selected from the 56-compound dataset described by (Hewitt et al., 2019) and are shown in Table 2. The criterion for selection was a melting point greater than 32°C. Unless otherwise noted, physical properties in Table 2 are those from the

Supplementary Table 1 in (Hewitt et al., 2019), supplemented by calculations of molar volume, V_A, density, ρ, and fraction unbound in a 2% albumin solution, f_u. In some cases, the solubility of a weak acid in water, S_w, was measured by CE at a pH where it is expected to be significantly ionized. For these compounds, the intrinsic (i.e. nonionized) S_w was taken from other sources as noted in the table. The pH dependent solubility was then estimated by standard methods (Sinko, 2011).

Dose information and the distribution of the compounds following a 24 h topical application to excised human surgical skin mounted in Franz diffusion cells are shown in Table 3. These data were extracted from the more extensive tables provided by (Hewitt et al., 2019) and (Gregoire et al., 2019). % evaporated is calculated as (100 – Mass balance) as in (Gregoire et al., 2019).

We supplemented the CE dataset with cysteine and lysine Direct Peptide Reactivity Assay (DPRA) and Perioxidase/peroxide-activated Peptide Reactivity Assay (PPRA) data from (Hoffmann et al., 2022), kinetic DPRA (kDPRA) log k_{max} values from (Natsch et al., 2020), murine Local Lymph Node (LLNA) EC3 values from (OECD, 2021), and also with chemical reactivity and skin sensitization predicted classifications from TIMES-SS (Oasis-LMC, 2024; Patlewicz et al., 2007). These data were used to develop a three-level classification scheme for identifying whether test compounds fall within the scope of DigiSkin 4.2. The classification scheme is shown in Table 4. The data and subsequent classifications may be found in Table S4 in the SI.

Table 2

CE solids dataset taken from (Hewitt et al., 2019). Properties listed are those from the original reference unless otherwise noted.

Compound	CAS No.	MW	V_A[a]	ρ[b]	mp,	pK_a[c]	Donor soln		Intrinsic S_w, 32°C	S_v, 32°C	log $K_{o/w}$	$P_{vp,sol}$,[d] 25°C
		g/mol	cm^3/mol	g/cm^3	°C		f_{non}	f_u[e]	mg/mL	mg/mL		mmHg
2-(Acetylamino)fluorene	53-96-3	223.27	238	1.161	194		1	0.13	0.004	9.7	3.12	4.80E-08
2,4-Dichloroacetophenone	937-20-2	189.04	175	1.330	101		1	0.06	0.63	0.6	2.27	1.70E-03
2,4-Dinitrochlorobenzene	97-00-7	202.55	157.5	1.519	50		1	0.55	0.41	0.4	2.17	8.48E-05
2,5-Diaminotoluene sulfate	615-50-9	122.17	140	1.070	64	5.98 BH+	0.913	0.90	7.9	7.9	0.2	3.41E-03
2-Aminophenol	95-55-6	109.13	119	1.154	174	4.74 BH+	0.993	0.83	20	20.0	0.62	5.01E-04
2-Nitro-p-phenylenediamine	5307-14-2	153.14	147	1.348	138	4.36 BH+	0.997	0.85	0.96	1.0	0.53	3.32E-05
4-Amino-3-nitrophenol	610-81-1	154.12	140	1.407	152		0.995	0.81	1.99	2.0	0.41	3.53E-05
4-Aminophenol	123-30-8	109.13	119	1.173	189	5.28 BH+	0.050	0.92	16.7[f]	350[i]	0.04	4.00E-05
4-Bromophenyl isocyanate	2493-02-9	198.02	143.5	1.535	42		1	0.51	0.04	11.4	3.48	9.60E-02
4-Nitro-o-phenylenediamine	99-56-9	153.14	147	1.345	201		1	0.85	0.21	0.2	0.88	6.93E-06
6-Methylcoumarin	92-48-8	160.17	161	1.180	76		1	0.10	0.49	0.5	1.91	5.12E-04
7-Ethoxycoumarin	31005-02-4	190.19	189	1.205	90		1	0.08	0.78	0.8	2.3	9.60E-05
Benzoic acid	65-85-0	122.12	126	1.156	122	4.2 HA	0.002	0.68	4.30[g]	4.5	1.87	7.00E-04
Benzophenone	119-61-9	182.22	203	1.098	48		1	0.10	0.22	0.2	3.18	1.93E-03
Benzylideneacetone	122-57-6	146.19	175	1.005	40		1	0.55	2.13	2.1	2.07	1.24E-02
C.I. Basic Red 76	68391-30-0	371.9	395.5	1.314	950		0	0.07	9.05	9.0	-0.32	2.12E-15
Caffeine	58-08-2	194.19	189	1.301	237		1	0.91	28.3[h]	17.5	-0.07	9.00E-07
Cinnamyl alcohol	104-54-1	134.17	161	1.007	33		1	0.71	3.98	4.0	1.95	2.40E-02
Cyclophosphamide monohydrate	6055-19-2	279.1	272.5	1.347	52		1	0.30	8.09	8.1	0.63	4.40E-05
Dimethyl fumarate	624-49-7	144.12	147	1.101	103		1	0.26	80	80.0	0.22	3.00E-01
HC Red No. 3	2871-01-4	197.19	196	1.291	128	3.88 BH+	1	0.80	3.65	3.7	0.51	7.19E-08
Helional	1205-17-0	192.21	196	1.151	77		1	0.74	0.34	0.3	2.51	8.03E-04
Hydrocortisone	50-23-7	362.47	406	1.300	220		1	0.58	0.41[g]	0.968	1.61	2.44E-10

Hydroquinone	123-31-9	110.11	112	1.238	173		1	0.90	59.32	59.3	0.59	2.40E-05
Ibuprofen	15687-27-1	206.28	252	0.991	76	4.41 HA	0.003	0.11	0.025[g]	0.409	3.97	1.86E-04
IQ	76180-96-6	198.22	196	1.282	300	5.15 BH+	0.973	0.26	0.53	0.5	1.47	5.61E-08
Methylisothiazolinone	2682-20-4	115.16	105	1.310	44		1	0.79	537	537.0	-0.83	2.93E-02
Methylparaben	99-76-3	152.15	154	1.197	127	8.31 HA	0.953	0.57	2.34	2.3	1.96	2.10E-05[j]
Naphthalene	91-20-3	128.17	154	1.15	81		1	0.08	0.03	320.2	3.3	8.51E-02[k]
p-Chloroaniline	106-47-8	127.57	129.5	1.211	70	3.97 BH+	0.999	0.63	3.25	3.2	1.83	2.70E-02
p-Phenylenediamine	106-50-3	108.14	126	1.113	142	6.17 BH+	0.871	0.90	8.28	8.3	-0.3	6.55E-04
Propylparaben	94-13-3	180.2	196	1.112	98	8.23 HA	0.944	0.50	0.52	0.5	3.04	8.06E-06[j]
Resorcinol	108-46-3	110.11	105	1.237	111	9.45 HA	0.996	0.89	504	503.7	0.8	4.89E-04
Testosterone	58-22-0	288.4	350	1.256	155		1	0.23	0.029[g]	106.2	3.32	1.70E-08
Thiram	137-26-8	240.4	238	1.461	155		1	0.41	0.12	1.5	1.73	1.73E-05
trans-Cinnamic acid	140-10-3	148.16	161	1.124	135	4.34 HA	0.002	0.17	0.79	0.8	2.13	5.00E-05
Triclosan	3380-34-5	289.5	248.5	1.199	57	7.8 HA	1	0.05	0.04	468.2	4.76	4.65E-06
Vanillin	121-33-5	152.15	154	1.199	83	7.78 HA	0.858	0.78	8.46	8.5	1.21	2.77E-04[l]

[a] Molar volume at the normal boiling point by Schröder's method (Poling et al., 2001)

[b] Density at 32°C

[c] Only relevant values are shown

[d] Experimental or calculated value from EpiSuite MPBPWin v1.44 (US_EPA, 2011) except as noted. For 32°C values, see Table S2.

[e] Calculation based on ACD Labs value of K_a^{HSA} assuming a 2% (0.6 mM) albumin solution according to $f_u = \left[1 + (6 \times 10^{-4}) K_a^{\mathrm{HSA}}\right]^{-1}$

[f] Experimental value from CompTox database (US_EPA, 2024)

[g] 25°C value from PubChem (PubChem, 2022) after correction to 32°C.

[h] Extrapolated from (Cesaro et al., 1976)

[i] Calculated from S_w and pK_a for an aqueous vehicle pH of 4.0, as reported in Supplemental Table 3 to (Hewitt et al., 2019)

[j] Extrapolated from (Verevkin et al., 2023)

[k] EpiSuite value confirmed by (Ambrose et al., 1975) and (Fowler et al., 1968)

[l] Estimated from (Almeida et al., 2019)

Table 3

Test conditions and experimental results for in vitro permeation test (IVPT) studies conducted by (Hewitt et al., 2019). The % distribution of the applied dose in various compartments was measured at the conclusion of the 24h study.

Compound	Dose	Vehicle	Initial pH	Fume hood?	Skin Wash	SC	ED	DE	Total Receptor	Mass Balance	Calc Evap[a]
	μg/cm^2				%	%	%	%	%	%	%
2-(Acetylamino)fluorene	1.30	100% ethanol	ND	No	86.29	2.39	0.82	1.02	4.37	94.90	5.10
2,4-Dichloroacetophenone	0.78	0.01M PBS	7.80	Yes	6.15	0.66	0.16	0.09	18.49	25.59	74.41
2,4-Dinitrochlorobenzene	4.26	0.1M PBS	7.20	No	10.27	1.73	9.88	2.64	50.04	74.56	25.44
2,5-Diaminotoluene sulfate	0.94	0.01M PBS+AOs	7.00	No	77.14	2.53	2.87	1.00	10.76	94.30	5.70
2-Aminophenol	5.85	0.1M PBS	7.00	No	37.39	3.33	2.36	1.05	45.80	89.93	10.07
2-Nitro-p-phenylenediamine	5.78	0.01M PBS	6.90	No	63.56	1.47	2.26	0.55	30.91	98.75	1.25
4-Amino-3-nitrophenol	11.76	0.01M PBS	6.90	No	51.82	3.48	2.98	0.79	38.18	97.20	2.80
4-Aminophenol	4.48	0.01M PBS+AOs	4.00	Yes	82.77	2.12	2.24	0.91	6.91	94.94	5.06
4-Bromophenyl isocyanate	1.24	100% ethanol	ND	No	72.32	17.13	1.93	0.51	0.36	92.24	7.76
4-Nitro-o-phenylenediamine	1.18	0.01M PBS	ND	No	45.58	4.21	4.11	1.51	40.91	96.32	3.68
6-Methylcoumarin	4.21	0.01M PBS	ND	No	3.12	0.14	0.04	0.02	93.89	99.84	0.16
7-Ethoxycoumarin	1.13	0.01M PBS	ND	No	5.84	0.20	0.09	0.11	91.70	97.97	2.03
Benzoic acid	7.92	0.01M PBS	ND	No	54.70	2.15	0.77	0.30	33.49	91.41	8.59
Benzophenone	1.28	0.01M PBS	7.30	No	4.40	0.25	0.05	0.07	68.38	73.16	26.84
Benzophenone	0.99	100% ethanol	NA	No	21.17	0.75	0.18	0.39	24.08	45.51	54.49
Benzylideneacetone	3.91	0.01M PBS	ND	No	6.44	1.45	1.48	0.62	70.27	80.27	19.73
C.I. Basic Red 76	53.27	0.01M PBS	ND	No	96.25	0.90	0.13	0.01	0.07	97.37	2.63
Caffeine	1.08	0.01M PBS	ND	No	54.05	2.06	1.02	0.52	39.46	97.11	2.89
Cinnamyl alcohol	6.72	0.01M PBS	ND	No	4.21	0.06	0.08	0.05	87.09	91.49	8.51
Cyclophosphamide monohydrate	47.42	0.1M PBS	ND	No	83.22	3.36	3.32	0.49	6.48	96.88	3.12
Dimethyl fumarate	6.24	0.1M PBS	5.00	No	4.65	0.62	0.52	0.25	18.05	24.09	75.91
HC Red No. 3	22.04	0.01M PBS	ND	No	90.33	3.67	1.44	0.08	1.26	96.82	3.18
Helional	2.63	0.01M PBS	7.00	Yes	13.66	2.28	0.24	0.22	60.94	77.34	22.66

Hydrocortisone	5.53	0.01M PBS	6.70	No	89.45	5.81	1.44	0.19	1.27	98.16	1.84
Hydrocortisone	5.41	100% ethanol	NA	No	81.75	6.23	3.36	1.19	1.12	93.65	6.35
Hydroquinone	15.73	0.01M PBS	7.00	No	57.59	9.80	10.06	1.08	14.30	92.85	7.15
Ibuprofen	2.51	0.01M PBS	ND	No	75.19	4.56	1.22	0.68	20.30	101.95	0
IQ	3.21	0.01M PBS	6.70	No	73.66	15.87	8.01	0.45	0.62	98.61	1.39
Methylisothiazolinone	13.62	0.01M PBS	7.00	No	6.08	1.02	6.11	2.87	45.91	62.00	38.00
Methylparaben	3.21	0.01M PBS	ND	No	16.79	0.29	0.14	0.23	76.78	94.24	5.76
Naphthalene	0.93	100% ethanol	ND	Yes	12.25	0.73	0.14	0.06	14.12	27.30	72.70
p-Chloroaniline	5.08	0.01M PBS	7.00	Yes	38.30	0.98	0.26	0.14	19.31	59.00	41.00
p-Phenylenediamine	0.91	0.01M PBS	7.00	No	53.53	9.39	8.81	1.83	8.20	81.75	18.25
Propylparaben expt. 1	2.42	0.01M PBS	ND	No	17.87	1.51	0.21	0.23	75.22	95.04	4.96
Propyl paraben expt. 2	2.51	0.01M PBS	ND	No	29.79	1.13	0.40	0.45	65.39	97.10	2.90
Propylparaben-expt. 2	2.96	100% ethanol	NA	No	73.33	0.69	0.32	0.44	10.26	85.03	14.97
Resorcinol	97.86	0.01M PBS	ND	No	17.09	5.23	2.97	1.15	70.06	96.51	3.49
Testosterone	1.64	100% ethanol	NA	No	85.99	4.13	0.80	0.48	3.43	94.83	5.17
Thiram	1.21	100% ethanol	ND	No	76.05	3.39	1.64	0.53	2.26	83.87	16.13
trans-Cinnamic acid	1.62	0.1M PBS	7.00	No	71.75	2.87	1.53	0.73	21.77	98.66	1.34
Triclosan	1.81	100% ethanol	NA	No	77.80	11.97	2.25	0.89	1.38	94.28	5.72
Vanillin	3.30	0.01M PBS	ND	No	21.17	1.73	0.28	0.18	55.94	81.76	18.24

Table 4
Rules for determining Digiskin 4.2 reliability scores and scope

Score[a]	Reactivity	Criteria
0 (out of scope)	high	CYS/LYS depletion in DPRA or PPRA Cysteine -/+ HRP/P ≥ 90 AND/OR experimental LLNA EC3<1 (Strong) AND/OR chemical contains 3 conjugated rings (highly planar)
1 (intermediate)	Medium	No experimental data but TIMES predicted Strong AND/OR CYS/LYS depletion in DPRA or PPRA Cysteine -/+ HRP/P = 70-90
2 (in scope)	Weakly or nonreactive	Remaining chemicals (not score 0 or 1)

[a] For brevity, reliability score will also be referred to as "Class".

3.2 Base model assumptions and parameters

With the exceptions noted in Sects. 3.3, the parameters employed in the present analysis were those used to simulate the CE liquids (Tonnis et al., 2022). The fully hydrated skin option (h_{sc} = 43.3 μm, H_{trans} = H_{lat} = 1) was selected for all calculations involving an aqueous dose solvent, and the partially hydrated skin option (h_{sc} = 13.4 μm, H_{trans} = H_{lat} = 3) was selected for calculations with an ethanol solvent. The reasoning behind the choice of skin hydration model was described in Sects. 3.2 and 4.1 of (Tonnis et al., 2022).

As with the CE liquids, it was assumed that both solvent and solute were uniformly dispersed on the skin surface as a well-stirred solution or suspension until the final stage of dry down (vehicle thickness h_v < 25 μm), after which lateral transport in the vehicle was not allowed, preventing unrealistically high accumulation of solute in the hair follicles (Yu et al., 2022). The receptor fluid (RF) was considered to be a perfect sink. The pH of the vehicle and the SC was allowed to vary as described in Sect. 2.3 and the pH of the ED and DE was assumed to remain constant at 7.4 throughout the experiment.

The default Model 3 and 4.0 values for wind velocity of u = 0.10 and 0.50 m/s were employed for simulating benchtop and fume hood experiments, respectively. However, the

related evaporative mass transfer coefficient, k_g, for all experiments was taken to be the optimized value from the CE liquids analysis (Tonnis et al., 2022), i.e. it was reduced from the Model 4.0 default value by the multiplier, $\bar{\alpha}_g$ = 0.080, estimated from the apparent evaporation rates of the solutes in the CE liquids dataset. Notably, we did *not* attempt to conduct further optimization of $\bar{\alpha}_g$, as the vapor pressures of the test compounds are already complicated by a correction related to the solid and subcooled liquid forms, cf. Eq. (6). This uncertainty, combined with the additional complexity related to dissolution rates of solids precipitated on the skin surface described in Sect. 2.1 were the primary reason for separating liquids and solids in our analysis of the (Hewitt et al., 2019) dataset.

3.3 Weak electrolytes

The pH recovery rate constant, k_r was estimated in a manner similar to (Tonnis et al., 2024). For that analysis, the composite parameter $a_0\beta_{sc}$ was optimized to fit finite dose applications of benzoic acid and propranolol over a wide range of dose sizes and initial pH, yielding a value of 20 nmol·cm^{-2}h^{-1}. Although strong acids and bases applied to skin react a bit differently, as discussed in (Tonnis et al., 2024), the same parameter was used for both cases due to insufficient evidence of a significant difference. To calibrate the model to the CE dataset, the buffer capacities of the 13 weak electrolytes listed in Table 2 were calculated and the composite parameter $a_0\beta_{sc}$ was allowed to vary to yield an optimum fit to the receptor fluid kinetics for these compounds. The optimized value $a_0\beta_{sc}$ = 60 nmol·cm^{-2}h^{-1} was used for the remainder of the analysis, yielding pH recovery rates about three-fold faster than those estimated by (Tonnis et al., 2024). Details are presented in Table S5 in the SI.

4. Results

4.1 Prediction reliability based on chemical reactivity

The accuracy of the DigiSkin dermal delivery predictions decreased with increasing chemical reactivity (Fig. 2). Only 16 compounds of the 38 were fully within the scope of the DigiSkin 4.2 model (weakly or nonreactive, reliability score 2), 7 compounds were on the border (moderately reactive, reliability score 1) and 15 compounds lay outside the scope (strongly reactive, reliability score 0).

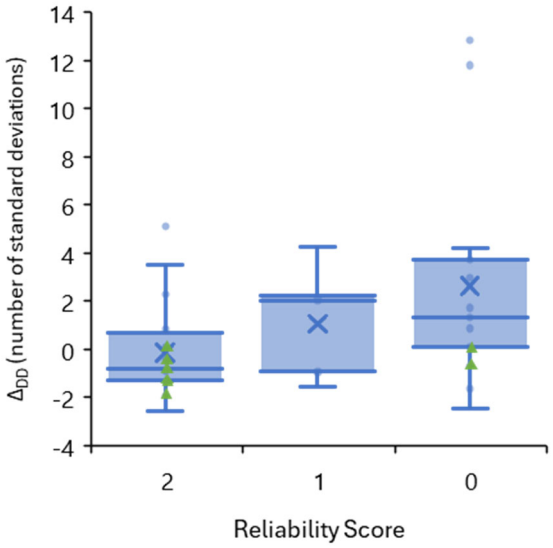

Fig. 2. Box and whiskers plot of the number of standard deviations difference between the predicted and experimental DD values (Δ_{DD}) for solutes dosed in PBS (circles) and EtOH (triangles). Reliability scores of 2, 1 and 0 correspond to compounds that are weakly or nonreactive, moderately reactive and highly reactive according to the classification scheme described in Sects. 3.1 and 5.2.3. X's denote means, horizontal lines denote 25th, 50th and 75th percentiles.

4.2 Evaporated amounts

Predicted evaporation of the nonreactive (Class 2) test compounds in the CE solids dataset is shown in Fig. 3, plotted vs the missing radioactive dose in the IVPT study (Table 3). Negative calculated evaporation was treated as 0% evaporated. A systematic error can be seen in Fig. 3

as the evaporation of the most volatile compounds tended to be overpredicted. Evaporation of compounds with very low volatility tended to be underpredicted. The latter could be due to other loss mechanisms in the experiments as well as volatility. The data in Fig. 3 are tabulated in Supplementary Table S7.

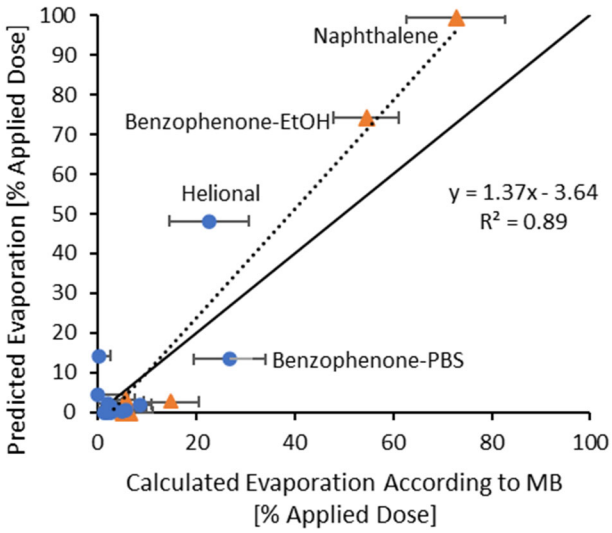

Fig. 3. Comparison of the predicted and measured evaporated fraction from the skin of weakly and nonreactive (Class 2) compounds according to Model 4.2. Chemicals dosed in PBS are represented as circles and those dosed in ethanol are represented as triangles. The dotted line represents a linear regression. The solid black line is the line of perfect fit.

4.3 Dermal delivery and skin surface retention of test solutes

Fig. 4 and 5 show a comparison of (a) the dermal delivery (DD) and (b) the skin surface retention of the test solutes after 24h in the CE experiments with those predicted using DigiSkin 4.2. As in the analysis of the CE liquids (Tonnis et al., 2022) and in Hewitt et al. (Hewitt et al., 2019), DD is defined as the sum of total amounts in the viable epidermis, dermis and receptor solution and skin surface retention is defined as the sum of amounts in the skin wash and stratum corneum (SC).

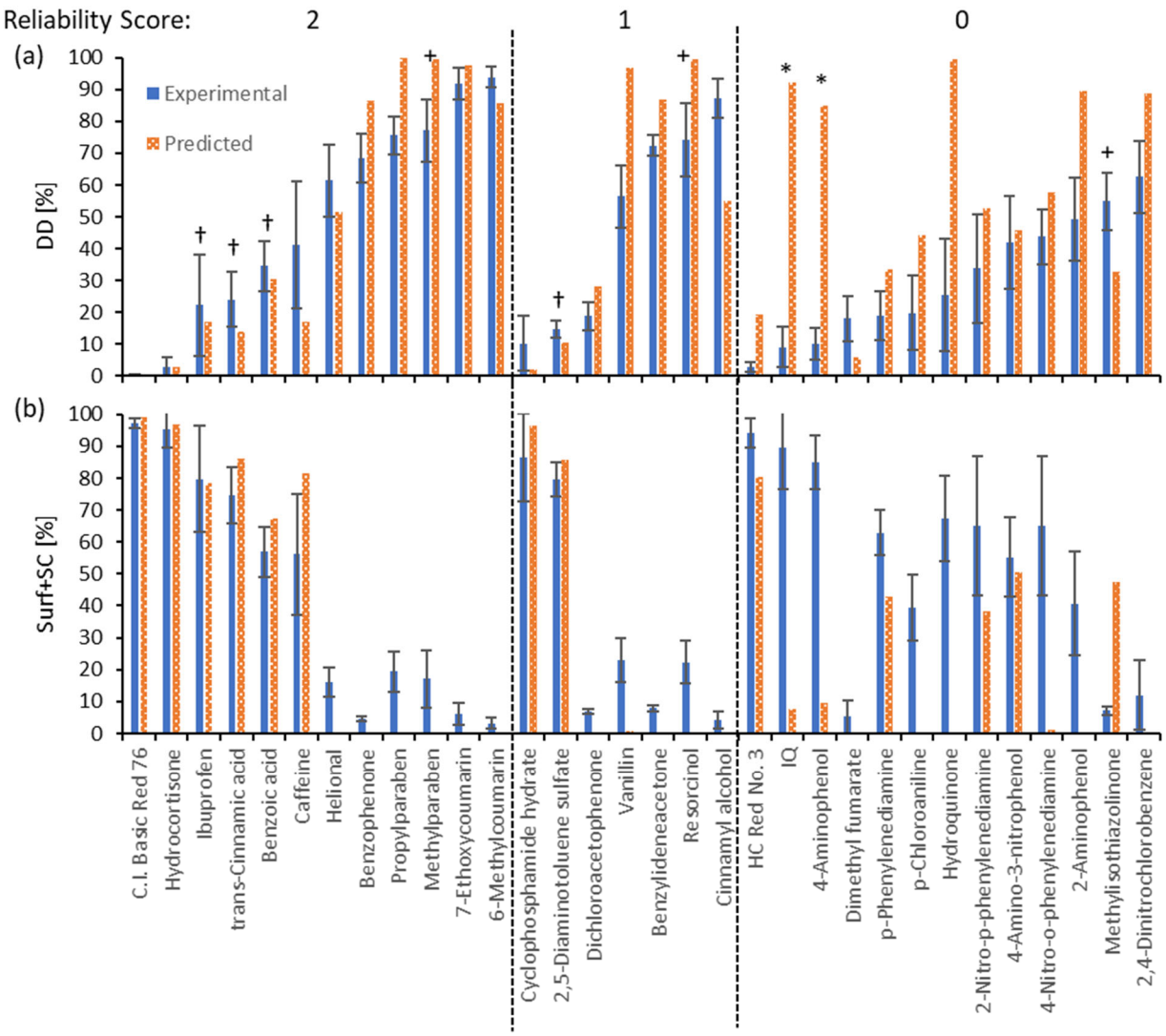

Fig. 4. Comparison of skin disposition after 24h for CE solids tested in PBS (solid blue) and simulated results using DigiSkin 4.2 (orange pattern). (a) Dermal delivery (ED + DE + receptor fluid); (b) Skin wash + SC. A "*" indicates a compound with uncertain physicochemical properties. A "+" indicates a compound with high water solubility. A "†" indicates a compound sensitive to skin pH. Error bars reflect the standard deviation of the summed values.

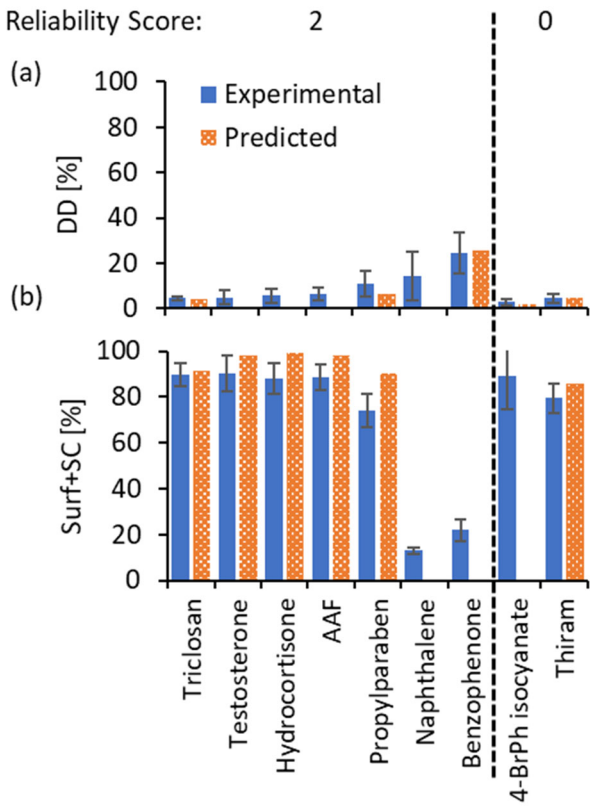

Fig. 5. Comparison of skin disposition after 24h for CE solids tested in ethanol. Panels, colors and symbols are the same as those in Fig. 4. There were no Class 1 compounds in this group.

For compounds tested in PBS, DD predictions for Class 2 compounds were within 2 SD of the observed values except for methyl and propyl paraben, which were overpredicted by slightly higher margins (Fig. 4a). In both cases the difference was due to precipitates that formed on the skin surface in the experiments. DD predictions for Class 1 compounds were on average within 4 SD. Although these predictions are less accurate than those for Class 2 compounds, they are still useful (Figs. 2 and 4a). Those for Class 0 compounds were less reliable, with 4 of 13 compounds being highly overpredicted. The overpredictions may be due to either chemical reactivity, uncertain physical properties or both, as discussed in Sect. 5.2.1.

Dermal delivery (DD) of compounds tested in ethanol was uniformly poor (Fig. 5a). DigiSkin 4.2 was able to match this phenomenon by means of the skin hydration and evaporation rate choices described in the Methods section. The difference between PBS and ethanol vehicles is remarkable, e.g. DD for benzophenone delivered from PBS was 68.5 ± 7.7 % of applied dose, whereas that from ethanol was 24.6 ± 9.1 % ((Hewitt et al., 2019). Factors leading to this difference are discussed in Sect. 5.1.

2-amino-3-methylimidazo[4,5-f]quinoline (IQ) is a potent mutagen that was largely found in the skin wash (74%) and SC (16%), whereas the model predicts that 92% will permeate to the receptor fluid. It was one of the compounds studied by Gregoire et al. using UV/Vis spectroscopy rather than a radiolabeled isotope. It intercalates to DNA but is only weakly reactive with peptides. To explain the poor penetration in the IVPT study, we speculate that its planarity formed a steric hindrance to penetration. An alternative hypothesis, discussed in Sect. 5.2.1, is that the water solubility or chemical purity of the test sample was not well characterized.

Two compounds in this dataset – methylisothiazolinone and resorcinol – are highly water soluble, which leads to problems with the dilute solution approximation employed in Models 4.0-4.2 (Tonnis et al., 2022). This assumption, which is equivalent to stating that partition coefficients are independent of concentration, is embodied (for example) in Eq. 1. However, the DD of methylisothiazolinone was only moderately underpredicted and that of resorcinol was moderately overpredicted. Issues with water solubility as well as other compounds with poorly predicted DD are discussed in Sect. 5.2.

Not surprisingly, skin surface retention showed an inverse relationship with DD. Compounds with underpredicted DD had overpredicted surface retention and vice versa. The high skin surface retention of all compounds dosed in ethanol except the volatile compounds naphthalene and benzophenone is notable. The impact of solvent dry down and ionization on skin surface retention is discussed in Sect. 5.2.3.

4.4 Receptor fluid kinetics

Plots of the predicted and experimental receptor fluid kinetics of each compound are shown in Supplementary Figs. S1 and S2. They correspond closely with the DD results in Figs. 4 and 5, as both experimental and predicted DD values were dominated by the 24 h receptor fluid amount. As with the liquids in the CE dataset (Tonnis et al., 2022) slowly reversible binding as presently parameterized had a modest impact on receptor fluid kinetics but did not appreciably affect the overall distribution of the compounds after 24 h (data not shown).

4.5 Impact of solid dissolution model

Fig. 6 shows a comparison of the predicted flux from the surface into the SC and the total mass of precipitated solid for 4-amino-3-nitrophenol using the hard solid dissolution model and the soft solid model. Plots of the predicted receptor fluid kinetics for each compound using the hard solid and soft solid approximation are shown in Supplementary Figs. S1 and S2. For most compounds dosed in PBS, the solid dissolution model made no difference because the dose was low enough to dissolve in the upper layers of the SC, i.e. the SC deposition zone (Tonnis et al., 2022), during solvent dry down and very little precipitated on the surface. Ethanol evaporates more quickly, and the compounds dosed in ethanol tended to have lower saturated concentrations in the SC deposition zone, leading to more solid precipitate on the skin surface.

Highly ionized weak electrolytes had decreased thermodynamic activity in the vehicle, which slowed their partitioning into the SC, leading to precipitation on the skin surface as the vehicle evaporated.

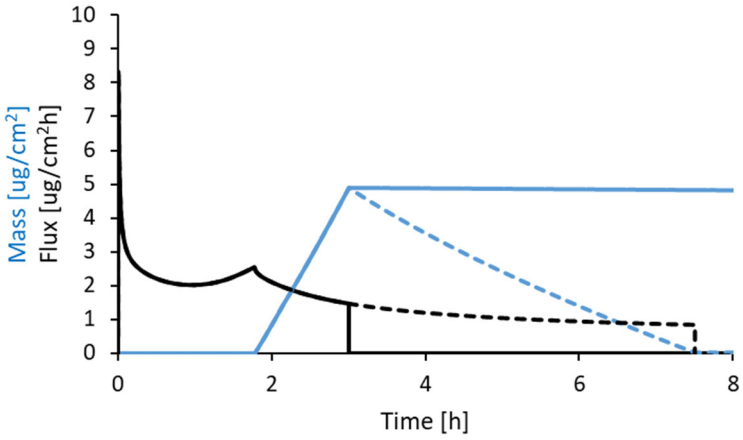

Fig. 6. Mass of solid on skin surface (blue) and flux from surface into the SC (black) for 4-amino-3-nitrophenol using a hard solid dissolution model (solid) and a soft solid dissolution model (dashes).

5. Discussion

The skin penetration dataset analyzed in this report (CE dataset) was first published in 2019 (Hewitt et al., 2019), but much of the data had been collected several years earlier. A number of research groups, including our own (GBK) had a look at the early data, but were unable to make much progress on an analysis with the tools available at that time. More recently, at least two full analyses ((Gregoire et al., 2021; Hamadeh et al., 2021)) and two partial analyses (Hamadeh et al., 2022; Tonnis et al., 2022) have appeared. These articles, as well as Hewitt's original publication, point out the complexity of this dataset and factors that must be considered in developing truly predictive methods for estimating the skin disposition of small doses of potentially volatile and often reactive organic chemicals. The present analysis further elucidates

these factors. We discuss below both experimental design and model considerations impacting dermal absorption and the prediction thereof for this complex dataset.

5.1 Experimental design

Two striking features of the CE dataset are the high impact of dose solvent on DD (PBS >> ethanol for 3 of 4 solutes) and the substantial percentage of many solutes found in the skin wash at very low doses that, according to simple solvent deposition models such as UB/UC (Dancik et al., 2013), should have been fully incorporated into the upper skin layers during the dry down process. In a recent analysis of the subset of the dataset that are liquids at skin temperature, we postulated that the extensive wash procedure employed by CE may have contributed to the high skin wash values (Tonnis et al., 2022). We subsequently tested this hypothesis and found it to be incorrect (Xu and Kasting, 2024). Rather, further testing pointed to rapid spreading and evaporation of the solvent from ethanolic dose solutions led to precipitation and/or evaporation of the solute before it could be absorbed into the skin. Pure water (a substitute for PBS for nonionizable solutes) had its own limitations as a delivery vehicle due to poor spreading on skin. Optimal simple delivery vehicles for maximizing absorption from low specific doses (13 $\mu L/cm^2$) without impacting skin permeability were ethanol/water mixtures and dilute aqueous nonionic surfactant solutions (Xu and Kasting, 2024).

The solvent differences in DD reported by (Xu and Kasting, 2024) were smaller than those reported by (Hewitt et al., 2019), suggesting that additional factors related to the dry down process may come into play. These factors are discussed in Sect. 5.2.

For IVPT testing of volatile compounds, many studies have been conducted employing either occlusion or vapor trapping to improve the mass balance. This is a sound design when the intention of the study is to provide a conservative (i.e. high) estimate of absorption for use in dermal risk assessment. However, if the intention of the study is to estimate absorption in realistic exposure scenarios, an unoccluded design is more appropriate. In this case the design and location of the diffusion cells in the laboratory are critical to the results obtained. As an example, the modest changes in these factors between our laboratory and the Eurofins laboratory where the CE finite dose permeation data were generated led to the need to decrease the default evaporation mass transfer coefficient in DigiSkin 4.2 by a factor of 12 to best fit the inferred evaporation associated with the Eurofins data (Tonnis et al., 2022). Rather than trying to standardize these variables across laboratories, a practical solution for interlaboratory comparisons would be to jointly characterize the evaporation of a chemically stable, moderately volatile organic liquid under standardized conditions. A potential reference compound is benzyl alcohol (Miller et al., 2006).

5.2 Model considerations

We continue here a discussion that begins in (Tonnis et al., 2022), which presented a detailed analysis of the 18 liquid compounds in the CE dataset. The focus will be on new considerations that either arose or became more important in the solids analysis. The reader is referred to the prior paper for a broader discussion of features of the DigiSkin dermal absorption model.

5.2.1 Physicochemical properties estimation

Key physicochemical properties determining dermal absorption in DigiSkin 4.2 and its predecessors include molecular volume (V_A), log octanol/water partition coefficient (log K_{ow} or logP), water solubility (S_w) and vapor pressure (P_{vp}). We employed measured properties whenever available. V_A and log K_{ow} can be either measured or readily estimated by several methods, and agreement between methods is pretty good. We employ Schroeder's Method for V_A due to its connection to aqueous diffusivity through the Wilke-Chang relationship (Poling et al., 2001) and (usually) EpiSuite measured values or predictions for log K_{ow}. In the present analysis the log K_{ow} values were those selected by (Hewitt et al., 2019).

Water solubility (S_w) is more difficult to accurately estimate, but it is readily measured in most laboratories. We used the values measured by (Grégoire et al., 2017) at the experimental temperature, 32^{o}C, and reported also in (Hewitt et al., 2019), except in the case of well-studied compounds where well accepted literature values exist. It is important for simulations of weak electrolytes that the S_w values input to the simulation software are those of the nonionized form, called herein the "intrinsic solublity", and that accurate pK_a values are also included as inputs. A puzzle in the present dataset is the true S_w value for 4-aminophenol, for which the value determined by Gregoire is much less than either literature experimental or predicted values for the compound or its isomer, 2-aminophenol. Gregoire et al. noted this in their analysis and expressed concern regarding the chemical stability of the 4-amino isomer. We have chosen to use the literature value of S_w for this compound. Its reactivity is discussed in the next section. The mutagen IQ was highlighted in the Results section as a compound with unusually poor skin penetration or DD. We tentatively assigned this result to the planarity of the structure and

resulting steric hindrance; however, there is scant literature support for this hypothesis. Napthalene, a planar bicyclic aromatic compound, penetrated better than DigiSkin 4.2 predictions in the present analysis. Alternative hypotheses to explain the poor penetration in the CE IVPT study include (1) it is more reactive in a thin film on skin than suggested by TIMES_SS or (2) it is less water-soluble than reported by Gregoire. It remains an outlier in our analysis. There is a growing body of research on the 5-ring polycyclic aromatic hydrocarbon benzo(a)pyrene and related compounds that may provide a clue to this puzzle (Bartsch et al., 2016; Bourgart et al., 2019).

Obtaining accurate vapor pressure (P_{vp}) estimates for the CE solids was the most problematical task in the present analysis, for several reasons: (1) P_{vp} is not readily measured in most chemistry laboratories, and the values reported by Gregoire et al. (Gregoire et al., 2019) and separately in (Hewitt et al., 2019) were mostly predicted values obtained from either EpiSuite (US_EPA, 2011) or CompTox (US_EPA, 2024). When we re-examined these sources, we found the predictions had changed. (2) P_{vp} estimation for solids is inherently more challenging than that for liquids because latent heat and heat capacity changes associated with melting must be considered as well as those for vaporization (Grain, 1990). Moreover, the extrapolations from the boiling point or triple point to either 25°C or skin temperature are often considerable. (3) Both solid ($P_{vp,sol}$) and subcooled liquid ($P_{vp,liq}$) vapor pressures become relevant in order to estimate evaporation of a dissolved solute that precipitates on the skin during dry down. Support for the concept that $P_{vp,liq}$ applies to dissolved solutes comes, for example, from gas chromatography (Haftka et al., 2006). (4) Some recently published, highly accurate vapor pressure measurements were not represented in the EpiSuite or CompTox databases. These

included values for methyl paraben, propyl paraben and vanillin. Significant differences from the predicted values were found.

We compared the 17 available experimental $P_{vp,sol}$ measurements for the CE solids dataset with predicted values from EpiSuite and with both mean and median predicted values from CompTox. The predictions from EpiSuite based on the modified Grain method yielded the best agreement and were selected for use in the analysis (for compounds lacking experimental data) following temperature and solid/liquid corrections.

Vapor pressure estimation of semi-volatile organic compounds is a long-standing problem in environmental science. Excellent discussions including descriptions of the methods employed in EpiSuite can be found in (Grain, 1990), (Woodrow et al., 2001), and (Stock et al., 2004) and references therein. Alternatives including SPARC (Hilal et al., 2003; Schossler et al., 2011) and COSMOtherm (Klamt, 2020) were not evaluated in this study.

5.2.2 Modeling the formulation dry down process

The present analysis highlights the difference between the initial one-component UB/UC model (Dancik et al., 2013) and the two-component DigiSkin 4.2 in simulating the solvent deposition process. In UB/UC volatile solvents evaporate immediately, depositing a portion of the solute (the saturation amount, M_{sat}) into the upper SC and the remainder on the skin surface. In partially hydrated skin, the top 10% of the SC is considered to be the "deposition layer" (Kasting and Miller, 2006). Thus, simple solvent systems such as ethanol, water or ethanol/water mixtures all yield the same results. In DigiSkin 4.2 the deposition layer concept is retained, but thermodynamic equilibrium of unbound solute and solvent between the vehicle phase and the

skin immediately following topical application is asserted in this region *without changing the partition properties of either phase.* The combination of these two assumptions leads to very different skin disposition of solutes dosed in water and water-miscible solutes such as ethanol. It offers a partial explanation for the large differences in permeation of solutes dosed in both solvents in the CE study, but it also sometimes misses the mark. Examples are shown in Fig. 7. The model predicts a large solvent effect on permeation for all three solutes, with absorption from PBS substantially greater than that from EtOH. This works well for benzophenone and propyl paraben, but fails for hydrocortisone, where the experimental values from both solvents were nearly identical.

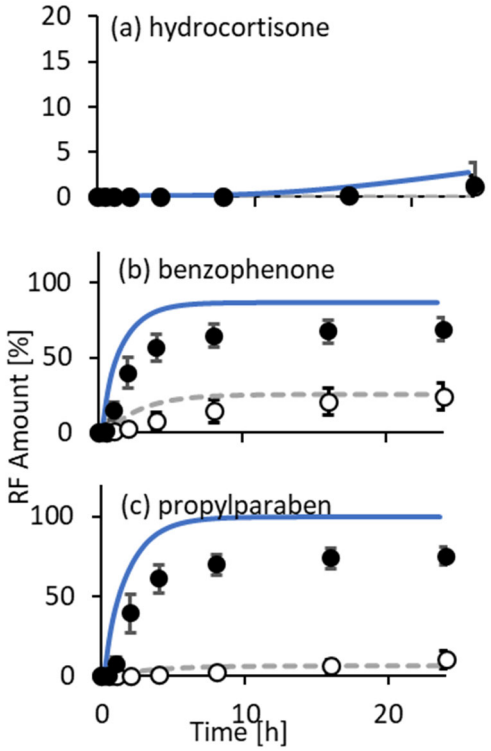

Fig. 7. RF amounts over time predicted by DigiSkin 4.2 with a PBS solvent (solid lines) and ethanol solvent (dashed lines) compared with experimental values in PBS (solid circles) and ethanol (open circles) for (a) hydrocortisone, (b) benzophenone and (c) propylparaben. Experimental values for hydrocortisone in PBS were nearly identical to those from ethanol and cannot be seen in the figure.

For volatile, lipophilic compounds dosed in ethanol, simulations with DigiSkin 4.2 become highly sensitive to the values selected for vapor pressure. Fig~~ure~~ 8 shows an example illustrating this phenomenon for the common preservative, propyl paraben. Using the default values for $P_{vp,liq}$ and $P_{vp,sol}$ estimated by EpiSuite, evaporation was greatly overpredicted. Inserting recent careful measurements of propyl paraben vapor pressure (Verevkin et al., 2023) greatly improved the agreement. UB/UC model predictions were much less sensitive to vapor pressure values, but substantially overpredicted the permeation from ethanol (data not shown).

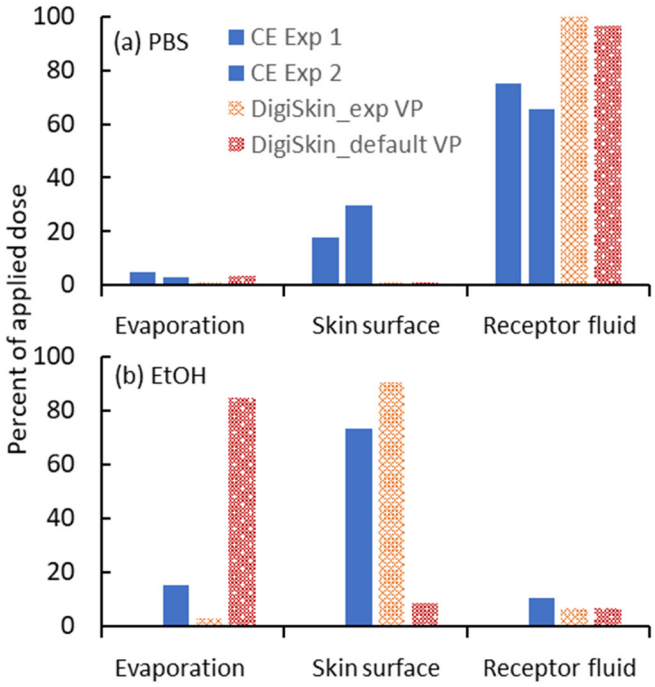

Fig. 8. Experimental and DigiSkin-predicted distributions of propyl paraben 24 h following application to skin in (a) PBS and (b) ethanol. The hard solid limit is shown. Amounts found in the skin layers were less than 2% of the dose and are not displayed. Predicted evaporation rates of propyl paraben from ethanol were highly sensitive to the selected vapor pressure, as discussed in the text; however, this factor had little impact on permeation into the receptor fluid for the simulations shown. A different result is obtained in the soft solid limit in which precipitated propyl paraben continues to penetrate the skin (Fig. S1). The experimental permeation data (Fig.7c) lie between these two limits, but are much closer to the hard solid.

Foreseeable improvements to the DigiSkin 4.2 dry down algorithm include the following:

(1) The SC deposition layer could be considered a separate compartment in the skin, having

properties different from the bulk SC. By imbuing it with higher diffusivity and allowing both vehicle and deposition layer composition to change due to exchange of solvent (from the formulation) and water (from the SC), more accurate solute partitioning and penetration rates into the skin could be estimated. (2) A more robust variation on this theme would be to allow the SC to swell differentially as in (Li et al., 2015), but with both water and organic solvent as coswelling agents. Strong support for this concept exists for the ethanol/water system (Berner et al., 1989a; Berner et al., 1989b). We encourage consideration of these concepts in order to improve the formulation "metamorphosis" aspect of transient dermal absorption models.

5.2.3 Effect of phase change on evaporation predictions

The capability to account for the difference in vapor pressure due to phase change during the dry down process implemented in DigiSkin 4.2 facilitates predictions of solids using a wide range of dose sizes and solvents. Solutes dosed in a highly volatile solvent such as ethanol spend most of their time on the surface as a solid, whereas those dosed in slower evaporating solvents spend more time in the dissolved state. In the DigiSkin 4.2 predictions, most compounds dosed in PBS had small enough doses to fully partition into the SC during dry down, so all predicted evaporation happened from the dissolved state. With larger or more concentrated doses, more solute would precipitate on the surface, increasing the impact of the variable vapor pressure.

5.2.4 Chemical reactivity

DigiSkin 4.2 will tend to overpredict the DD of reactive compounds because it does not have a mechanism to bind them to proteins in the skin, so they are free to penetrate or evaporate. A chemical reaction rate constant that correlates with retention on or within the skin is needed.

We examined reaction rate constant (k_{max}) in the kDPRA assay (Natsch et al., 2020), but were unable to confirm the relationship suggested in (Tonnis et al., 2022), possibly by not having enough data. kDPRA is a kinetic version of the Direct Peptide Reactivity Assay that is based on the time course of cysteine depletion under a prescribed concentration regimen. Results are shown in Fig. S5 in the SI. The proposed reliability scheme is not only useful in the current analysis but also in providing reliability of the future predictions.

5.2.5 Weak electrolytes

Weak electrolyte permeation was well handled by the mechanism introduced in (Tonnis et al., 2024) and described in Sect. 2.3; however, the SC buffer capacity providing the best fit to the data, as represented by $a_0\beta_{sc}$ (Eq. 9) was reduced by a factor of three in order to produce the best fit. This decision was based largely on the experimental permeation of the three weak acids in the solids dataset (benzoic acid, cinnamic acid and ibuprofen), which were much more sensitive to the value of $a_0\beta_{sc}$ than were the weak bases. This decision resulted in the calculated pH for the CE experiments approaching pH^{∞} (i.e. pH 5.5) three times as quickly as in (Miller and Kasting 2022). We note that, in contrast to the Miller and Kasting study, in which the only buffer in the dose solution was the weak acid or base itself, most of the dose buffer capacity in the CE study was due to the phosphate buffer (pK_2 = 7.2). Thus, the buffer capacity of the CE dose solutions was mostly due to soluble phosphate, whereas that for the weak acid in the Miller and Kasting study (benzoic acid, pK_a 4.19) was related to the solute, which precipitated on the skin as the dose increased.

The mechanistic framework for predicting the transient pH in the SC and vehicle introduced in Model 4.1 and carried over into Model 4.2 allowed for drastic improvement in predictions for solid weak electrolytes compared with the constant pH used in Model 4.0. Model 4.0 was suitable for short exposures or doses with buffer capacities large enough to ensure the pH stayed near the dose pH for the relevant time frame (Tonnis et al., 2022). Consequently, the RF kinetics of 4-chlorobutyric acid, 4-methylvaleric acid and thioglycolic acid could be predicted using constant pH because evaporation shortened the exposure time. The solid electrolytes in the CE dataset are on the surface longer, so RF predictions are sensitive to transient pH. Fig. 9 shows a comparison of the Model 4.2 RF predictions (transient pH described by Eqs. 7-9) with those of Model 4.0 (static pH) using either the dose pH or the skin pH of 5.5 as the static value.

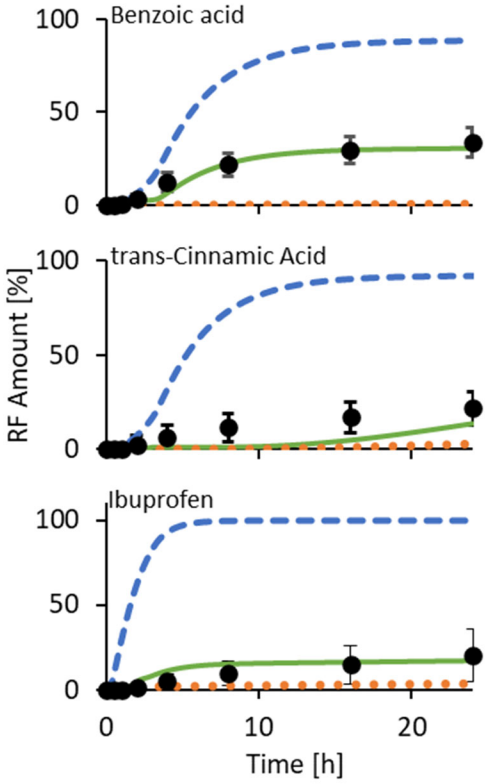

Fig. 9. Comparison of the predicted RF amounts using Model 4.2 (solid green), Model 4.0 with the dose pH (orange dots) and Model 4.0 at a pH of 5.5 (blue dashes). The symbols represent the CE measurements and their standard deviation.

The other weak electrolytes in the CE dataset are mostly nonionized at both the dose pH and pH 5.5, so the transient pH model did not have a noticeable effect on their RF predictions.

5.2.6 Solid dissolution on skin

Due to the low applied doses and the experimental considerations discussed in Sect. 5.1, we were not able to further test the dissolution model described in Sect. 2.1 and summarized in Eqs. (1) and (2). This model includes a dissolution mass transfer coefficient, κ_{lip}, for precipitated solid on the skin surface that was first introduced by (Yu et al., 2022). Instead, we present in Figs. S1 and S2 limits of no dissolution (hard solid) and instantaneous dissolution (soft solid) that bound the range of possibilities encompassed by Eqs. (1) and (2). For small doses of lipophilic compounds delivered from PBS there is usually no difference because the solute immediately partitions into the SC "deposition region" (Figs. S1-S3). However, for lipophilic compounds dosed from ethanol there is often a substantial difference (Fig. S4). In this case the hard solid approximation usually comes closer to the experimental data than does the soft solid approximation. Yet there is clear evidence for continued permeation of the solute well after the solvent has evaporated – see, for example, the RF kinetics profiles for 2-(acetylamino)fluorene, thiram, naphthalene, propyl paraben and testosterone in Fig. S4. This is why, as stated in Sect. 5.2.2, improvements in the dry down model are required in order to accurately explain these data. Thus, we have not given up the belief that Eqs. (1) and (2) or an improvement thereof are required to quantitatively describe the dissolution of solids on the skin.

6. Conclusions

The present study extended our previous analysis (Tonnis et al., 2022) of the skin disposition of small doses of cosmetically-relevant compounds as measured in an in vitro study (Hewitt et al., 2019). Whereas Tonnis et al. considered only the compounds that are liquid at skin temperature, we have now analyzed the solids. The DD of liquids and solids in this dataset followed many of the same trends. Model 4.2 predicted the DD of most solids within two standard deviations. Chemical reactivity, uncertainties in water solubility and equilibrium vapor pressure, and details of the formulation dry down algorithm were the biggest factors in causing the predictions to deviate from the experimental observations. Because of the size of the dose and the environmental conditions in the experiments, for many of the experiments most of the dose penetrated the skin before the solvent had evaporated, and they penetrated much like liquids. The addition of features to account for dissolution rate limitation on the flux of a solid from the surface of the skin provide an explanation for the slower, but measurable, penetration of solids when a significant part of the dose precipitated on the surface. Gradual drift of the SC pH back toward its natural value and the resulting neutralization of weak acids and bases deposited on the skin surface provides an explanation for their continued absorption into the skin.

CRediT author contribution statement

Kevin Tonnis: Investigation, Formal analysis, Visualization, Writing – Original draft; **Joanna Jaworska:** Funding acquisition, Supervision, Formal analysis, Review and editing; **Gerald B. Kasting:** Funding acquisition, Supervision, Formal analysis, Review and editing.

Declaration of interests

The authors declare that they have no known competing financial interests or personal relationships that could have appeared to influence the work reported in this paper.

Data availability

Algorithms are fully described in this article and its predecessors. Computational results are available in the Supplementary Information. The gPROMS computer code is the property of Procter & Gamble. However, predecessor models UB/UC and Model 2 may be accessed as MoBi applications in the Open Systems Pharmacology Suite, v11, available on GitHub, as described in (Hamadeh et al., 2019) and (Hamadeh and Edginton, 2023). The UB/UC model is furthermore available as the Finite Dose Skin Permeation Calculator, a downloadable Java application on the NIOSH/CDC website (Fedorowicz et al., 2011).

Acknowledgments

KT was supported by the Procter & Gamble Company. GBK was supported by a grant from the US National Science Foundation (NSF) GOALI program under grant number 2124495 (CBET). We thank Abdullah Hamadeh and Andrea Edginton for helpful conversations and for capably translating large portions of the developed codes into open access pharmacology software, as well as extending the capabilities of the model.

References

Almeida, A.R.R.P., Freitas, V.L.S., Campos, J.I.S., Ribeiro da Silva, M.D.M.C., Monte, M.J.S., 2019. Volatility and thermodynamic stability of vanillin. J. Chem. Thermodyn. 128, 45-54.

Ambrose, D., Lawrenson, I.J., Sprake, C.H.S., 1975. The vapor pressure of naphthalene. J. Chem. Thermodyn. 7, 1173-1176.

Anissimov, Y.G., Roberts, M.S., 2001. Diffusion modeling of percutaneous absorption kinetics: 2. Finite vehicle volume and solvent deposited solids. J. Pharm. Sci. 90, 504-520.

Bartsch, N., Heidler, J., Vieth, B., Hutzler, C., Luch, A., 2016. Skin permeation of polycyclic aromatic hydrocarbons: A solvent-based in vitro approach to assess dermal exposures against benzo[a]pyrene and dibenzopyrenes. J. Occup. Environ.Hyg. 13, 969-979.

Berner, B., Juang, R.-H., Mazzenga, G.C., 1989a. Ethanol and water sorption into stratum corneum and model systems. J. Pharm. Sci. 78, 472-476.

Berner, B., Mazzenga, G.C., Otte, J.H., Steffens, R.J., Juang, R.-H., Ebert, C.D., 1989b. Ethanol:water mutually enhanced transdermal therapeutic system II: skin permeation of ethanol and nitroglycerin. J. Pharm. Sci. 78, 402-407.

Bourgart, E., Barbeau, D., Marques, M., von Koschembahr, A., Beal, D., Persoons, R., Leccia, M.-T., Maitre, A., 2019. A realistic human skin model to study benzo[a]pyrene cutaneous absorption in order to determine the most relevant biomarker for carcinogenic exposure. Arch. Toxicol. 93, 81-93.

Cesaro, A., Russo, E., Crescenzi, V., 1976. Thermodynamics of caffeine aqueous solutions. J. Phys. Chem. 80, 335-339.

Dancik, Y., Miller, M.A., Jaworska, J., Kasting, G.B., 2013. Design and performance of a spreadsheet-based model for estimating bioavailability of chemicals from dermal exposure Adv. Drug Deliv. Revs. 65, 221-236.

Ellison, C.A., Tankersly, K.O., Obringer, C.M., Carr, G.J., Manwaring, J., Rothe, H., Duplan, H., Géniès, C., Grégoire, S., Hewitt, N.J., Jacques-Jamin, C., Klaric, M., Lange, D., Rolaki, A., Schepky, A., 2020. Partition coefficient and diffusion coefficient determinations of 50 compounds in human intact skin, isolated skin layers and isolated stratum corneum lipids. Toxicol. in Vitro 69, 104990.

Fedorowicz, A., Millller, M.A., Frasch, H.F., Kasting, G.B., 2011. Finite dose skin permeation calculator. NIOSH, http://www.cdc.gov/niosh/topics/skin/finiteSkinPermCalc.html.

Fowler, L., Trump, W.N., Vogler, C.E., 1968. Vapor pressure of naphthalene. J. Chem. Eng. Data, 209-210.

Grain, C.F., 1990. Sect. 14 Vapor pressure, in: Lyman, W.J., Reehl, W.F., Rosenblatt, D.H. (Eds.), Handbook of Chemical Property Estimation. McGraw-Hill, New York.

Gregoire, S., Cubberley, R., Duplan, H., Eilstein, J., Hewitt, N.J., Jacques-Jamin, C., Genies, C., Klaric, M., Rothe, H., Ellison, C., Fernandez, J., Schepky, A., 2019. Use of a simple in vitro test to assess Loss of chemical due to volatility during an in vitro human skin absorption study. Skin Pharmacol. Physiol. 32, 117-124.

Grégoire, S., Cubberley, R., Duplan, H., Eilstein, J., Lange, D., Hewitt, N., Jacques-Jamin, C., Klaric, M., Rothe, H., Ellison, C., Vaillant, O., Schepky, A., 2017. Solvent solubility testing of cosmetics-relevant

chemicals: methodology and correlation of water solubility to in silico predictions. J. Soln. Chem. 46, 1349-1363.

Gregoire, S., Sorrell, I., Lange, D., Najjar, A., Schepky, A., Ellison, C., Troutman, J., Fabian, E., Duplan, H., Genies, C., Jacques-Jamin, C., Klaric, M., Hewitt, N., 2021. Cosmetics Europe evaluation of 6 in silico skin penetration models. Comp. Toxicol. 19, 100177.

Haftka, J.J.H., Parsons, J.R., Govers, H.A.J., 2006. Supercooled liquid vapour pressures and related thermodynamic properties of polycyclic aromatic hydrocarbons determined by gas chromatography. J. Chrom. A 1135, 91-100.

Hamadeh, A., Edginton, A., 2023. Efficient large-scale mechanism-based computation of skin permeability. Comp. Toxicol. 26, 100263.

Hamadeh, A., Sevestre, M., Edginton, A.J., 2019. Implementation of Dancik et al (2013) skin permeation model in MoBi, https://github.com/Open-Systems-Pharmacology/Skin-permeation-model.

Hamadeh, A., Troutman, J., Edginton, A.J., 2021. Assessment of vehicle volatility and deposition layer thickness in skin penetration models. Pharmaceutics 13, 807.

Hamadeh, A., Troutman, J., Najjar, A., Edginton, A., 2022. A mechanistic Bayesian inferential workflow for estimation of in vivo skin permeation from in vitro measurements J. Pharm. Sci. 111, 838-851.

Hewitt, N.J., Grégoire, S., Cubberley, R., Duplan, H., Eilstein, J., Ellison, C., Lester, C., Fabian, E., Fernandez, J., Géniès, C., Jacques-Jamin, C., Klaric, M., Rothe, H., Sorrell, I., Lange, D., Schepky, A., 2019. Measurement of the penetration of 56 cosmetic relevant chemicals into and through human skin using a standardized protocol. J. Appl. Toxicol. 2019, 1-13.

Hilal, S., Karickhoff, S., Carreira, L., 2003. Prediction of the vapor pressure boiling point, heat of vaporization and diffusion coefficient of organic compounds. QSAR Comb. Sci. 22, 565–574.

Hoffmann, S., Alépée, N., Gilmour, N., Kern, P.S., van Vliet, E., Boislève, F., Bury, D., Cloudet, E., Klaric, M., Kühn, J., Lalko, J.F., Mewes, K., Miyazawa, M., Nishida, H., Brami, M.T., Varçin, M., Api, A.M., Cosmetics_Europe, 2022. Expansion of the Cosmetics Europe skin sensitisation database with new substances and PPRA data. Reg. Toxicol. Pharmacol. 131, 105169.

Kasting, G.B., Miller, M.A., 2006. Kinetics of finite dose absorption through skin 2. Volatile compounds. J. Pharm. Sci. 95, 268-280.

Kasting, G.B., Miller, M.A., LaCount, T.D., Jaworska, J., 2019. A composite model for the transport of hydrophilic and lipophilic compounds across the skin. J. Pharm. Sci. 108, 337-349.

Klamt, A., 2020. COSMOthermX, 5274M ed. Biovia Division, Dassault Systemes, Velizy-Villacoublay, France, p. Solution thermodynamics program.

Li, X., Johnson, R., Weinstein, B., Wilder, E., Smith, E., Kasting, G.B., 2015. Dynamics of water transport and swelling in human stratum corneum. Chem. Eng. Sci. 138, 164-172.

Miller, M.A., Bhatt, V., Kasting, G.B., 2006. Absorption and evaporation of benzyl alcohol from skin. J. Pharm. Sci. 95, 281-291.

Miller, M.A., Kasting, G.B., 2022. Absorption of solvent-deposited weak electrolytes and their salts through human skin in vitro. Int. J. Pharm. 620, 121753.

Natsch, A., Haupt, T., Wareing, B., Landsiedel, R., Kolle, S., 2020. Predictivity of the kinetic direct peptide reactivity assay (kDPRA) for sensitizer potency assessment and GHS subclassification. ALTEX 37, 652-664.

Nitsche, J.M., Kasting, G.B., 2022. A framework for incorporating transient solute-keratin binding into dermal absorption models. J. Pharm. Sci. 111, 2093-2106.

Oasis-LMC, 2024. OASIS-LMC\TIMES 2.32.1. Oasis Laboratory of Mathematical Chemistry, Bourgas, Bulgaria.

OECD, 2021. Annex 3: Report of the sub-group on the curation and evaluation of the local lymph node assay reference data and the derivation of associated substance classifications according to the UN GHS, in: Committee, E.D.C.a.B. (Ed.). Organization for Economic Cooperation and Development, Paris.

Patlewicz, G., Dimitrov, S.D., Low, L.K., Kern, P.S., Dimitrova, G.D., Comber, M.I.H., Aptula, A.O., Phillips, R.D., Niemelä, J., Madsen, C., EWedebye, v.B., Roberts, D.W., Bailey, P.T., Mekenyan, O.G., 2007. TIMES-SS—A promising tool for the assessment of skin sensitization hazard. A characterization with respect to the OECD validation principles for (Q)SARs and an external evaluation for predictivity. Reg. Toxicol. Pharmacol. 48, 225-239.

Poling, B.E., Prausnitz, J.M., O'Connell, J.P., 2001. The properties of gases and liquids, 5th ed. McGraw-Hill, New York.

PubChem, 2022. PubChem. National Institutes of Health.

Scheuplein, R.J., Ross, L.W., 1974. Mechanism of percutaneous absorption V. Percutaneous absorption of solvent deposited solids. J. Invest. Dermatol. 62, 353-360.

Schossler, P., Schripp, T., Salthammer, T., Bahadir, M., 2011. Beyond phthalates: Gas phase concentrations and modeled gas/particle distribution of modern plasticizers. Sci. Total Environ. 409, 4031-4038.

Sinko, P.A., 2011. Martin's Physical Pharmacy and Pharmaceutical Sciences, 6th ed. Lippincott Williams & Wilkins, Philadelphia, PA.

Stefaniak, A.B., Harvey, C.J., 2006. Dissolution of materials in artificial skin surface film liquids. Toxicol. in Vitro 20, 1265-1283.

Stock, N.L., Ellis, D.A., Deleebeeck, L., Muir, D.C.G., Mabury, S.A., 2004. Vapor pressures of the fluorinated telomer alcohols -- limitations of estimation methods. Environ. Sci. Technol. 38, 1693-1699.

Tonnis, K., Jaworska, J.S., Kasting, G.B., 2024. Modeling the percutaneous absorption of solvent-deposited solids over a wide dose range: II. Weak electrolytes. J. Control. Rel. 365, 435-447.

Tonnis, K., Nitsche, J.M., Xu, L., Haley, A., Jaworska, J.S., Kasting, G.B., 2022. Impact of solvent dry down, vehicle pH and slowly reversible keratin binding on skin penetration of cosmetic relevant compounds: I. Liquids. Int. J. Pharm. 624, 122030.

US_EPA, 2011. Estimation Programs Interface Suite™ vers. 4.11. U.S. Environmental Protection Agency, Washington, DC, USA, for Microsoft® Windows.

US_EPA, 2024. CompTox Chemicals Dashboard v2.3.0. United States Environmental Protection Agency, Washington, D.C.

Verevkin, S.P., Zaitsau, D.H., Emel'yanenko, V.N., Varfolomeev, M.A., Nagrimanov, R.N., 2023. Review on thermochemistry of parabens: evaluation of experimental data with complementary measurements, structure–property correlations and quantum chemical calculations. J. Thermal Anal. Calorim. 148, 13709–13727.

Woodrow, J.E., Seiber, J.N., Dary, C., 2001. Predicting pesticide emissions and downwind concentrations using correlations with estimated vapor pressures. J. Agric. Food Chem. 49, 3841−3846.

Xu, L., Kasting, G.B., 2024. Solvent and crystallization effects on the dermal absorption of hydrophilic and lipophilic compounds. J. Pharm. Sci. 113, 948-960.

Yu, F., Tonnis, K., Kasting, G.B., Jaworska, J., 2021. Computer simulation of skin permeability of hydrophobic and hydrophilic chemicals: Influence of follicular pathway. J. Pharm. Sci. 110, 2149-2156.

Yu, F., Tonnis, K., Xu, L., Jaworska, J., Kasting, G.B., 2022. Modeling the percutaneous absorption of solvent-deposited solids over a wide dose range. J. Pharm. Sci. 111, 769-779.